EAI Endorsed Transactions
on Scalable Information Systems

Research Article EAI.EU

Data-Model Hybrid-Driven Multi-Timescale Low-Carbon Economic Dispatch for Manufacturing-Park Virtual Power Plants

Ruosong Hou*, Wei Guo, Ziheng Zhao, Xiaolin Tan, Yuan Cao

State Grid Hebei Electric Power Research Institute, Shijiazhuang, Hebei Province, China

Abstract

INTRODUCTION: Manufacturing parks combine energy-intensive production equipment, auxiliary systems, distributed renewables, and flexible loads, creating coupled fluctuations between production schedules and electricity demand.
OBJECTIVES: This study develops an auditable data-model hybrid method that links empirically updated uncertainty scenarios with a production-constrained, low-carbon, three-stage dispatch model for manufacturing-park virtual power plants.
METHODS: The data module estimates wind-speed, irradiance, manufacturing-load, and price distributions from rolling historical records, generates joint scenarios, and updates operating states. The model module solves a coupled day-ahead-intraday-real-time stochastic program with process-feasibility, carbon-flow, storage, and inter-park constraints; reduced scenarios and measured deviations form the interface between the two modules.
RESULTS: Case studies show a 22.6% reduction in operating cost, an 18.0% reduction in carbon emissions, a renewable-energy absorption rate of 94.8%, and a 48.8% reduction in power-fluctuation standard deviation compared with single-time-scale dispatch.
CONCLUSION: The proposed framework coordinates energy and production decisions while maintaining production feasibility and improves economic, low-carbon, and operational performance under high renewable penetration.

Keywords: Manufacturing park; virtual power plant; multi-timescale dispatch; low-carbon economic dispatch; production scheduling; uncertainty quantification

Received on 05 July 2026, accepted on 11 August 2026, published on 26 August 2026

doi: 10.4108/eetsis.13894

*Corresponding author. Email: houruosong@126.com

1. Introduction

1.1. Background and Motivation

Manufacturing is a major energy-consuming and carbon-emitting sector, and integrating energy performance into production management has become essential for cost control and sustainable competitiveness. In manufacturing parks, continuous processes, batch production, compressed-air systems, industrial HVAC, electric heating, and on-site renewable generation create coupled fluctuations between production schedules and electricity demand. Large-scale wind and photovoltaic integration introduces additional uncertainty into distribution networks, while traditional load-following dispatch cannot simultaneously accommodate renewable volatility, production continuity, and market-price changes. Flexible distributed-resource coordination is therefore required.

Manufacturing-park virtual power plants (MP-VPPs) use communication, industrial internet, and control technologies to aggregate rooftop photovoltaics, distributed generation, battery storage, utility systems, and flexible production loads. Equipped with power regulation and peak-shaving functions, MP-VPPs can mitigate renewable-energy fluctuations and coordinate factory electricity demand. Unlike general demand response, manufacturing-load regulation must respect process sequence, equipment availability, product quality, and delivery constraints. Since renewable output, production load, and electricity prices exhibit different characteristics across time scales, a single-time-scale model cannot reliably coordinate production and energy resources. Therefore, constructing a multi-time-scale collaborative optimization model for MP-VPPs is of significant practical necessity.
Theoretically, addressing uncertainty quantification, multi-stage model construction, low-carbon objectives, and multi-agent coordination in MP-VPP dispatch can enrich the framework of production-energy collaborative optimization. Precise uncertainty quantification provides reliable input data, multi-timescale coordination unifies operational objectives, and carbon-flow calculation together with production-aware demand response expands the optimization dimensions. Practically, the optimized model can reduce manufacturing energy cost and carbon intensity while maintaining production continuity. The day-ahead stage aligns energy procurement with production schedules, the intraday stage corrects forecast and order deviations through rolling optimization, and the real-time stage coordinates storage, compressed-air systems, HVAC, charging facilities, and noncritical process loads. The model therefore serves as a decision-support tool linking manufacturing energy management, production planning, and grid dispatch.

1.2. Related Work

Reviews and case studies have shown that virtual-power-plant aggregation, stochastic scheduling, model-predictive control, and hierarchical energy management can coordinate distributed generation, storage, and flexible loads under high renewable penetration [1-6]. For manufacturing parks, industrial edge-computing platforms, integration of energy-efficiency performance into production management, and production-oriented energy key performance indicators provide the data and management basis for linking dispatch decisions with production execution [7-9].
Related research has used probabilistic scenario assessment, bi-level stochastic scheduling, Gaussian-process wind-power forecasting, stochastic-robust optimization, and probability-metric scenario reduction to represent renewable-output, source-load, and forecast uncertainties [10-14]. These methods improve scenario representation, but most do not simultaneously model production-order changes, equipment availability, and utility-system cycling across day-ahead, intraday, and real-time horizons.
Low-carbon virtual-power-plant and carbon-aware power-system research has introduced carbon-emission-flow accounting, marginal or time-varying emission factors, joint energy-reserve-carbon markets, electricity-carbon joint trading, and data-driven low-carbon dispatch [15-19]. However, the allocation of embedded emissions from purchased electricity and on-site generation to specific production and auxiliary systems remains insufficiently represented in manufacturing-park applications.
Demand response and coordinated operation have been addressed through market-based demand response, game-theoretic scheduling, agent-based VPP coordination, peer-to-peer energy sharing, benefit allocation, and multi-energy-carrier coupling [20-25]. Existing studies nevertheless tend to represent industrial demand as generic flexible load and rarely impose process sequence, shift windows, minimum operating time, delivery deadlines, and rebound constraints in a unified scheduling model.
Recent work has advanced multi-time-scale VPP scheduling by representing storage degradation and heterogeneous user flexibility [26], combining scenario generation with stochastic-robust optimization [27], and integrating artificial intelligence with production-oriented demand response [28]. These studies demonstrate the value of richer uncertainty and industrial-load models, but they generally optimize energy flexibility, production execution, or carbon allocation as separate layers rather than as a single auditable day-ahead-intraday-real-time workflow.
Three gaps therefore remain. First, existing data-driven VPP studies seldom identify the exact interface through which fitted distributions, scenario probabilities, and online measurements enter a constrained dispatch model. Second, generic elastic-load formulations do not guarantee process precedence, delivery deadlines, equipment availability, setup time, minimum run time, interruption limits, and rebound completion. Third, most carbon-aware multi-timescale studies do not transfer source-tagged carbon consistently through storage, exports, curtailment, and inter-park exchange. The proposed framework addresses these gaps jointly and treats production feasibility as a hard condition rather than a post-optimization check.

1.3. Main Contributions

The novel contribution is distilled into the following three points:
(1) An explicit data-model hybrid architecture. The data-driven module fits stage-specific uncertainty distributions, constructs probability-weighted joint scenarios, and updates states from metering and manufacturing-execution-system records. The model-based module enforces network, storage, carbon, market, and production constraints. Scenario trajectories and probabilities flow downward to optimization, while realized deviations, storage states, and production progress flow upward for rolling re-estimation.
(2) A coupled three-stage production-energy formulation. Day-ahead commitment, intraday rolling recourse, and real-time tracking are linked by non-anticipativity, state continuity, frozen-decision, and energy-aggregation rules. Unlike elasticity-only demand response, the formulation

includes process precedence, deadlines, minimum run time, equipment availability, setup, interruption, recovery, and rebound constraints together with source-tagged carbon accounting for purchased power, storage, exports, curtailment, and inter-park exchange.
(3) A manufacturing-oriented validation and reproducibility protocol. The two-park case evaluates economic cost, operational carbon, renewable absorption, fluctuation suppression, and process feasibility under deterministic, stochastic, robust, and literature-based multi-time-scale benchmark definitions. The revised protocol reports data processing, scenario reduction, probability calculation, solver tolerances, convergence criteria, and the exact input plots required for independent replication.

2. Manufacturing-Park Virtual Power Plant Structure and Multi-Time-Scale Dispatch Implications

2.1. Manufacturing-Park Virtual Power Plant Structure

The core function of an MP-VPP is to aggregate and coordinate energy resources embedded in a manufacturing park. A typical system contains rooftop photovoltaics and wind power, controllable distributed generators, battery energy storage, production and utility loads, and an integrated energy-management system [1,2,6,7]. Renewable resources reduce purchased electricity but introduce weather-driven volatility and forecast uncertainty [5,10,12,13]. Controllable generators such as gas turbines or combined heat and power units provide dispatchable support [1,17,25]. Battery storage absorbs surplus renewable energy and supplies peak demand [4,5,26]. Manufacturing loads are divided into critical, shiftable, and utility loads. Critical production processes cannot be interrupted; shiftable processes can move within permitted time windows; utility systems such as compressed air, industrial HVAC, chilled water, electric boilers, and charging facilities can provide faster demand response [20-23,28]. The energy-management system exchanges data with the manufacturing execution system, collects energy and production information, predicts demand, solves dispatch decisions, and issues coordinated control instructions.
When several manufacturing parks are interconnected through smart-grid and industrial-internet platforms, they form a multi-park MP-VPP system. As shown in Figure 1, renewable generation, controllable generation, battery storage, and electrical and manufacturing loads are linked to the central energy-management system through bidirectional information and control channels. The central platform collects operating data, performs forecasting and optimization, and issues coordinated dispatch commands to each resource. Compared with isolated operation, this hierarchical structure enables coordinated energy exchange, reserve sharing, higher renewable-energy utilization, and improved supply reliability while preserving the autonomy of each manufacturing park [4,22,24,25].

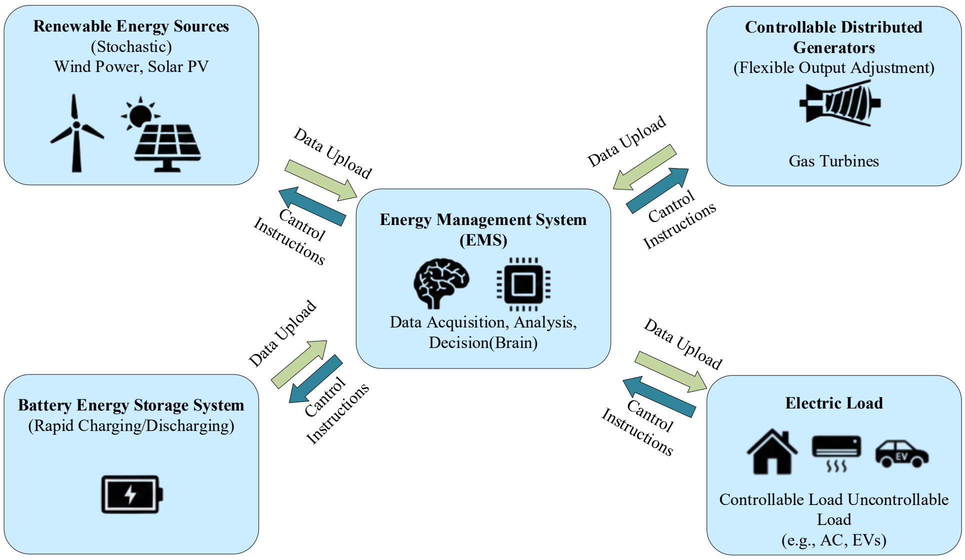

Figure 1. Block diagram of the structure and composition of a manufacturing-park virtual power plant

2.2. Division and Characteristics of Multi-Time-Scale Dispatch

The division of multi-timescale scheduling for MP-VPPs depends on renewable and production-load uncertainty, the decision horizon, and the response speed of different resources. Scheduling is divided into day-ahead, intraday, and real-time stages, each corresponding to distinct production-planning information and energy-control capabilities.

Day-ahead scheduling operates at a 1-hour time scale over a 24-hour horizon. It formulates generation, electricity purchase/sale, storage charging/discharging, and flexible manufacturing-load plans based on the next day's production schedule, shift calendar, renewable forecast, load forecast, and electricity-price forecast. Its objective is to minimize operating cost and carbon emissions while meeting production volume, process sequence, equipment, and energy-balance constraints. Because day-ahead decisions affect subsequent stages, sufficient reserve capacity and load-shifting margins must be retained for forecast errors and production changes.

Intraday scheduling uses 15-minute or 30-minute intervals and rolling horizons of 4 or 6 hours. It updates the day-ahead plan using ultra-short-term renewable forecasts, real-time metering, production progress, equipment status, and order adjustments. This stage corrects deviations without changing critical production sequences, coordinates storage and flexible utility systems, and keeps both the park power balance and the manufacturing schedule within allowable limits.

Real-time dispatch operates at 5-minute or 10-minute intervals and addresses instantaneous fluctuations in renewable output and manufacturing demand. Fast resources such as battery storage, compressed-air systems, industrial HVAC, charging facilities, and selected noncritical loads are adjusted to maintain power balance and power quality. Critical processes and quality-sensitive equipment are excluded from emergency curtailment. The objective is to minimize real-time operating and deviation-penalty costs while satisfying grid instructions and production-safety constraints.

Day-ahead scheduling establishes the baseline energy plan corresponding to the production plan; intraday scheduling corrects the baseline through rolling optimization; and real-time scheduling suppresses residual fluctuations. Figure 2 illustrates this sequential relationship: the day-ahead stage forms an hourly reference plan, the intraday stage revises it using updated forecasts and production progress, and the real-time stage performs fast tracking and balance control. Real-time operating results, storage states, and production progress are then fed back to the upper stages, forming a closed-loop coordination mechanism that hierarchically mitigates uncertainty and links energy dispatch with manufacturing execution.

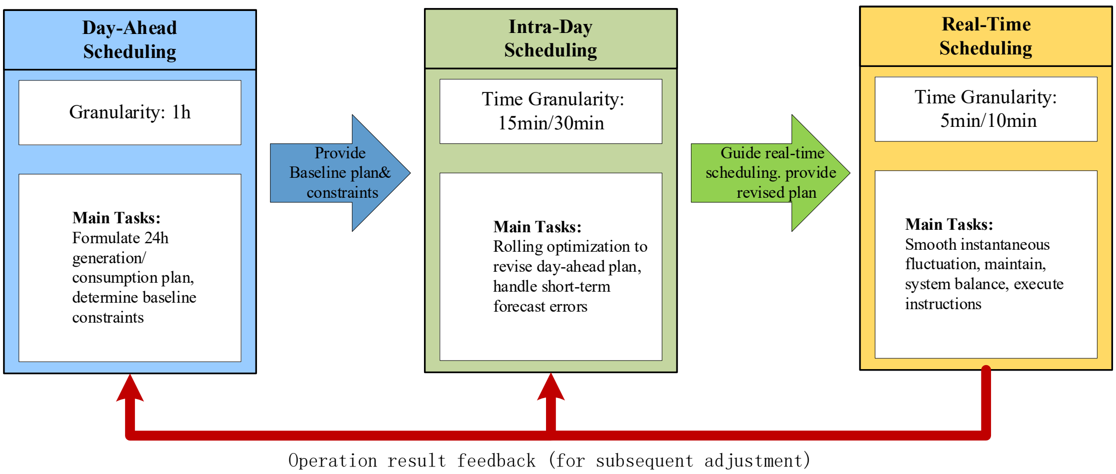

Figure 2. Manufacturing-Park Virtual Power Plant Multi-Time-Scale Scheduling Framework

2.3. Core Objectives and Constraints of Multi-Time-Scale Scheduling

2.3.1. Core Objectives

The core objective of MP-VPP multi-timescale scheduling is to coordinate economic efficiency, low-carbon performance, renewable-energy integration, and production continuity while ensuring safe operation. Each time scale has a different focus, but all stages must remain consistent with the manufacturing plan.

Economic objectives include minimizing fuel, storage maintenance, electricity procurement, flexible-load regulation, and deviation-penalty costs, while also considering electricity-sales and ancillary-service revenue. For manufacturing parks, energy cost per unit of output and peak-demand charges are important operational indicators. Low-carbon objectives minimize emissions from on-site fuel consumption and purchased electricity through carbon-flow accounting. Renewable-energy integration is improved by coordinating storage, utility systems, and shiftable processes, provided that production quantity, delivery time, and product-quality constraints are satisfied.

2.3.2. Constraints

MP-VPP multi-timescale scheduling must satisfy system, equipment, production, and market constraints. Their effects differ across time scales and jointly determine the feasible region of manufacturing-oriented dispatch.

System constraints primarily include power balance and electrical safety. At every time step, the sum of distributed generation, grid exchange, and storage discharge must balance manufacturing and auxiliary-system demand together with storage charging. The equality constraint is expressed as follows:

$$P_{G,t} + P_{grid\_pur,t} + P_{ES\_disch,t} = P_{load,t} + PPG_{grid\_sales,t} + P_{ES\_chg,t} \quad (1)$$

In Equation (1), t is the dispatch-period index; PG,t is the output power of controllable distributed generators; Pgrid,pur,t is the power purchased from the utility grid; PES,disch,t is the battery-energy-storage discharging power; Pload,t is the total demand of production equipment and auxiliary systems; PPGgrid,sales,t is the power sold to the utility grid; and PES,chg,t is the storage charging power. All power variables are expressed in kW, and the equality requires total supply at period t to equal consumption, export, and charging demand.

Equipment constraints include output limits, ramping limits, and start-stop conditions for controllable generation; charging/discharging power, state of charge, and efficiency limits for storage; and availability limits for renewable generation. Flexible manufacturing loads additionally require shift-window, minimum run-time, process-sequence, maximum interruption, recovery, and production-volume constraints. For example, compressed-air and HVAC loads may respond rapidly within pressure or temperature bands, whereas a heat-treatment or continuous production line may only be shifted within a predefined scheduling window.

Market constraints define electricity purchase/sale volumes, bidding rules, and ancillary-service requirements for MP-VPP participation. Market commitments must remain compatible with available park flexibility and cannot compromise production delivery or equipment safety.

3. Quantitative Model for Multi-Time-Scale Uncertainty in Manufacturing-Park Virtual Power Plants

3.1. Identification and Classification of Uncertainty Factors

MP-VPP operation is affected by interacting uncertainties across different time scales. The main factors are renewable-energy output uncertainty, manufacturing electricity-load uncertainty, and electricity-price uncertainty. Production-order variation and equipment availability are reflected in the manufacturing-load forecast and its error distribution.

Renewable-energy output uncertainty is a major source of MP-VPP imbalance. Wind and solar generation depend on weather conditions, and forecast errors can create deviations between the energy plan and actual park operation. Day-ahead errors are generally larger because of the longer forecast horizon, whereas intraday and real-time forecasts are more accurate but still affected by abrupt weather changes. These deviations influence electricity procurement, storage operation, and the amount of manufacturing-load flexibility required.

Manufacturing electricity-load uncertainty arises from production schedules, order changes, machine start-stop states, batch transitions, utility-system cycling, ambient conditions, and operator decisions. Day-ahead forecasts rely on production plans and historical energy data; intraday forecasts are updated using manufacturing-execution and metering information; real-time demand still contains short-duration fluctuations caused by equipment operation. Inaccurate load prediction can increase peak demand, energy cost, and the risk of insufficient reserve capacity.

Electricity-price uncertainty is driven by market supply and demand, policy, fuel price, and renewable availability. Day-ahead, intraday, and real-time prices follow different formation mechanisms. Price uncertainty directly affects the energy procurement cost of manufacturing parks and the economic value of shifting production and utility loads.

3.2. Multi-timescale Uncertainty Quantification Method

To represent uncertainties at different time scales, the data module uses only observations available before each scheduling run. Positive physical drivers (wind speed and normalized irradiance) are modeled directly, whereas signed manufacturing-load and price forecast residuals are fitted separately. This distinction prevents a positive-support distribution from being incorrectly imposed on a signed forecast error.

3.2.1. Quantification of Renewable Energy Output Uncertainty

Wind speed v is nonnegative and is fitted with a Weibull distribution. The Weibull law is not imposed on the signed wind-power forecast error. Instead, sampled wind speeds are converted to available wind power through the turbine power curve and then combined with the point forecast, preserving the physical bounds $0 \le PWT \le PWT_{max}$. The probability density is:

$$f_v(v;k,c) = \frac{k}{c}\left(\frac{v}{c}\right)^{k-1} \mathrm{e}^{\left[-\left(\frac{v}{c}\right)^{k}\right]}, \quad v \ge 0 \quad (2)$$

In Equation (2), k and c are the dimensionless shape and wind-speed scale parameters estimated by maximum likelihood for each dispatch stage. Scenario wind power is obtained as PWT=g(v), where g(·) is the manufacturer power curve; this revision therefore distinguishes the wind-speed distribution from the induced wind-power error distribution.

For photovoltaic generation, the bounded variable x=PPV/PPV+ is defined on [0,1] and is fitted with a beta distribution. As with wind power, the beta law is applied to the normalized physical output rather than to an unrestricted signed residual. The density is:

$$f_x(x;\alpha,\beta)=\frac{x^{\alpha-1}(1-x)^{\beta-1}}{B(\alpha,\beta)},\quad 0\le x\le 1 \tag{3}$$

In Equation (3), x is normalized photovoltaic output, α and β are positive shape parameters, and $B(\alpha,\beta)=\frac{\Gamma(\alpha)\Gamma(\beta)}{\Gamma(\alpha+\beta)}$. Samples are mapped back through $PPV=xPPV_{+}$ and truncated at the stage-specific available capacity. Zero-output nighttime periods are modeled as a point mass and are excluded from continuous beta-parameter estimation.

3.2.2. Quantification of Manufacturing Electricity Load Uncertainty

Manufacturing-load residuals $\varepsilon L=PL,actual-PL,forecast$ are signed. A normal distribution is retained only when the stage-specific residual sample passes the diagnostic procedure in Section 3.2.4; otherwise the best supported Laplace, Student-t, or empirical distribution is used. For the normal candidate:

$$f(\varepsilon_L;\mu_L,\sigma_L)=\frac{1}{\sqrt{2\pi}\sigma_L}\exp\left[-\frac{(\varepsilon_L-\mu_L)^2}{2\sigma_L^2}\right] \tag{4}$$

In Equation (4), μL and σL are the residual mean and standard deviation estimated separately for day-ahead, intraday, and real-time horizons. Residuals are conditioned on shift, production mode, and equipment-availability indicators before aggregation so that order changes are not hidden inside an undifferentiated error term.

3.2.3. Quantification of Electricity Price Uncertainty

Electricity-price residuals $\varepsilon_\rho=\rho_{\text{actual}}-\rho_{\text{forecast}}$ are also signed. Normal, Laplace, Student-t, and empirical candidates are compared by the same out-of-sample diagnostics; the normal candidate is:

$$f(\varepsilon_\rho;\mu_\rho,\sigma_\rho)=\frac{1}{\sqrt{2\pi}\sigma_\rho}\exp\left[-\frac{(\varepsilon_\rho-\mu_\rho)^2}{2\sigma_\rho^2}\right] \tag{5}$$

In Equation (5), μ_ρ and σ_ρ are the mean and standard deviation of the stage-specific price residual. Prices are reconstructed as $\rho=\rho_{\text{forecast}}+\varepsilon_\rho$ and truncated only at market-imposed bounds. Separate models are fitted for day-ahead, intraday, and real-time markets to avoid pooling different price-formation mechanisms.

3.2.4. Historical-Data Fitting and Goodness-of-Fit Validation

For each simulated operating day, the fitting window contains only earlier forecast and measurement records. Missing intervals are removed, outliers caused by confirmed meter faults are excluded using maintenance logs, and the remaining series are resampled to the target stage resolution. Parameters are estimated by maximum likelihood; beta variables are normalized to [0,1], and zero-inflated photovoltaic samples are fitted with a mixed point-mass/continuous model.

Candidate families are Weibull, gamma, lognormal, and empirical distributions for wind speed; beta, Kumaraswamy, and empirical distributions for normalized photovoltaic output; and normal, Laplace, Student-t, and empirical distributions for load and price residuals. Model ranking uses Akaike and Bayesian information criteria on the fitting sample, followed by Kolmogorov-Smirnov and Anderson-Darling tests and quantile-coverage error on a chronologically later validation block. A parametric family is retained only when it is not rejected at the 5% level and improves validation coverage; otherwise bootstrap sampling from the empirical residual distribution is used.

This procedure is repeated for each dispatch horizon and season. Thus, Weibull, beta, and normal laws are case-study selections supported by a transparent test protocol, not universal assumptions. The data module exports the selected distribution, estimated parameters, validation statistics, and timestamped training window to the optimization module for auditability.

3.3. Uncertainty Handling Based on Scenario Generation and Reduction

To integrate quantified uncertainty into multi-timescale regulation decision models, scenario generation and reduction techniques are employed. These convert continuous probability distributions into a finite set of discrete scenarios, each corresponding to specific values and occurrence probabilities of uncertainty factors. Scenario generation comprehensively reflects potential variations in uncertainty factors, while scenario reduction minimizes scenario count and simplifies model solution complexity without compromising computational accuracy.

3.3.1. Scenario Generation

Based on the fitted marginal models, 1,000 joint Monte Carlo trajectories are generated for each day-ahead update. Temporal and cross-variable dependence among wind, photovoltaic output, manufacturing load, and price is preserved through the rank-correlation matrix of the fitting window; intraday and real-time trees are conditioned on observations available at the rolling-update instant. A fixed seed is stored for every experiment so the scenario set can be regenerated exactly.

3.3.2. Scenario Reduction

The initial trajectories are standardized by their physical ranges before distance calculation so that price or load scale cannot dominate the reduction. A probability-aware fast-forward procedure retains 10 day-ahead, 6 intraday, and 5 real-time representative scenarios. Each discarded trajectory is assigned to its nearest retained trajectory, and the retained probability equals the sum of the original probabilities in that cluster.

For candidate scenarios i and j, the standardized Manhattan distance is:

$$d_{ij}=\sum_k\left|\frac{x_{ik}-x_{jk}}{R_k}\right| \tag{6}$$

In Equation (6), R_k is the observed or engineering range of factor k. If C_s denotes the set of original trajectories assigned to retained scenario s, its probability is $\pi_s = \sum_{i \in C_s} \pi_i$, with $\pi_s \geq 0$ and $\sum_s \pi_s = 1$. Decisions at nodes sharing the same information history satisfy non-anticipativity, preventing the optimizer from using future observations. The complete procedure is summarized in Figure 3.

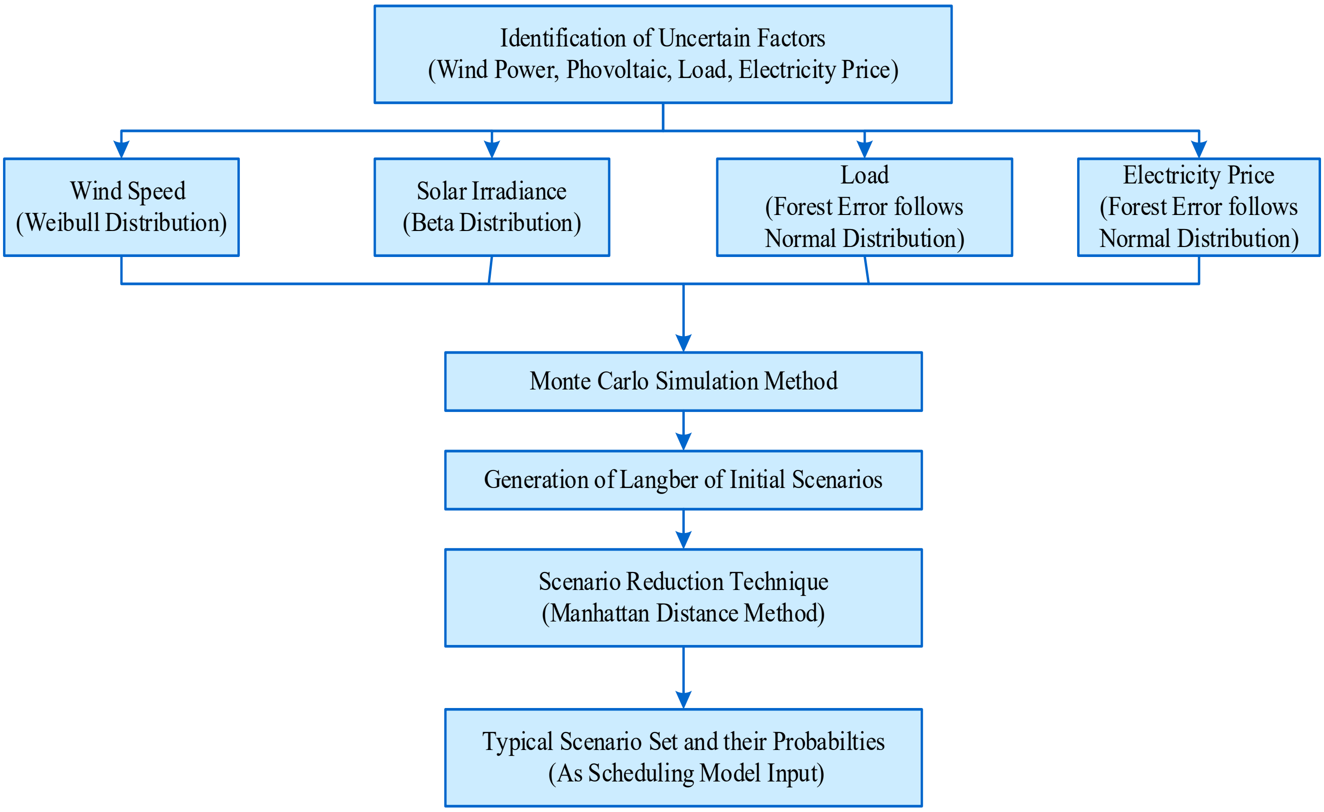

Figure 3. Flowchart of Manufacturing-Park Uncertainty Scenario Generation and Reduction

4. Optimization of Multi-Time-Scale Regulation Decision Models for Manufacturing-Park Virtual Power Plants

4.1. Overall Framework for Model Optimization

The overall MP-VPP framework has two auditable engines connected by a timestamped interface. The data engine ingests forecasts, measurements, production orders, equipment states, and market records; fits and validates uncertainty models; generates and reduces joint scenarios; and returns scenario trajectories, probabilities, and confidence diagnostics. The model engine receives those outputs and solves the day-ahead, intraday, and real-time production-energy problems. Metered deviations, realized prices, storage states, machine availability, and remaining production quantities are fed back to the next data update, closing the hybrid loop.

The data input layer collects renewable and electricity-price forecasts, production orders, shift calendars, equipment operating states, manufacturing-load forecasts, storage and generator parameters, flexible-load windows, market rules, and carbon-emission data. These inputs connect the energy-management system with the manufacturing execution system and determine the accuracy of optimization results.

The uncertainty processing layer employs the multi-timescale uncertainty quantification model and scenario generation/reduction techniques proposed herein to address uncertainties in input data. It generates scenario sets for each timescale, providing reliable inputs for the multi-stage dispatch layer.

The multi-stage scheduling layer is the core of the model. Day-ahead scheduling coordinates energy procurement and the planned production profile; intraday rolling optimization responds to updated orders, equipment status, and forecasts; real-time control uses metering and production-state data to maintain instantaneous balance. Data feedback and command transmission maintain consistency among the three stages.

The output layer produces distributed-generation schedules, storage charging/discharging plans, grid transaction plans, and control instructions for utility systems and flexible production loads, thereby guiding both park energy operation and production-side response. Figure 4 summarizes the complete four-layer framework: forecast, production, equipment, market, and carbon data enter the data-input layer; uncertainty models and scenario reduction form the processing layer; day-ahead, intraday, and real-time optimization constitute the scheduling layer; and executable energy and production commands are generated in the output layer. The feedback path in Figure 4 returns actual operating and production information to the upper layers so that subsequent decisions can be corrected online.

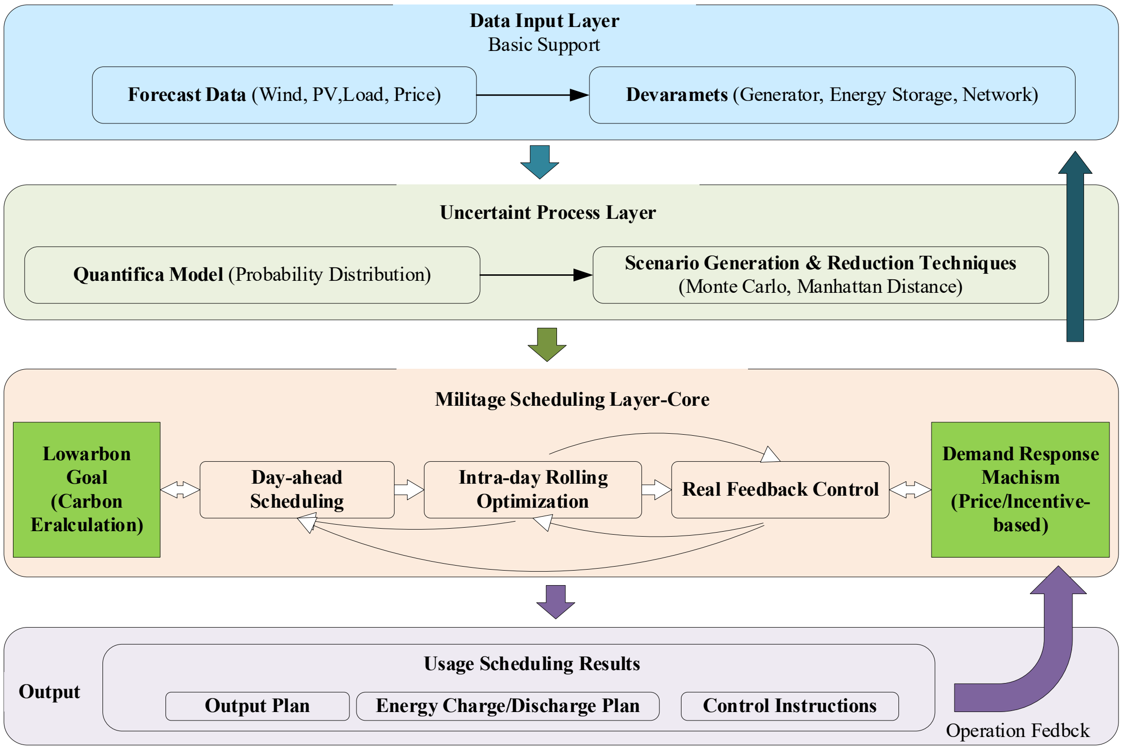

Figure 4. Overall Framework for Multi-Time-Scale Production-Energy Regulation Decision Optimization

4.2. Optimization of the Day-Ahead-Intraday-Real-Time Three-Stage Regulation Decision Model

4.2.1. Sets, Variables, and Information Structure

Let S_τ be the scenario set at stage $\tau \in \{DA, ID, RT\}$, $\pi_{s\tau}$ the probability of scenario s, and H, Q, and R the day-ahead, intraday, and real-time periods. First-stage variables include generator commitment/start-up, hourly grid exchange, storage baseline, reserve, and process-start decisions. Intraday variables revise dispatchable output, storage, utilities, and not-yet-started flexible processes. Real-time variables are limited to fast storage, utility, charging, and approved noncritical-load actions. State variables include storage energy, unit status, machine availability, cumulative production, and remaining process flexibility.

4.2.2. Day-Ahead Stochastic Scheduling

The day-ahead problem minimizes expected operating and carbon cost over 24 hourly periods while reserving flexibility for lower stages:

$$\min F^{\mathrm{DA}} = \sum_{s\in S^{\mathrm{DA}}} \pi_s \sum_{h\in H} \left[C^{G} + C^{\mathrm{grid}} + C^{\mathrm{ES}} + C^{\mathrm{DR}} + c_{\mathrm{CO_2}} E + c^{\mathrm{cur}} P^{\mathrm{cur}} \right] \tag{7a}$$

Subject to every scenario's power balance, generator commitment and ramping, purchase/sale limits, storage state transition and terminal SOC, renewable availability, reserve, carbon budget, and production constraints in Section 4.3. The scenario probabilities enter the objective explicitly, while commitment and process-start variables before uncertainty revelation satisfy non-anticipativity.

4.2.3. Intraday Rolling Recourse

At each 15-minute update, a 4-hour receding horizon minimizes incremental operating cost and deviation from the feasible day-ahead baseline:

$$\min F^{\mathrm{ID}} = \sum_{s\in S^{\mathrm{ID}}} \pi_s \sum_{q} \left[C^{\mathrm{inc}} + \lambda^{\mathrm{DA}} \left| P^{\mathrm{ID}}_{\mathrm{grid},q} - \bar{P}^{\mathrm{DA}}_{\mathrm{grid},h(q)} \right| \right] \tag{7b}$$

Completed or quality-critical process decisions are fixed; only the remaining feasible production window is re-optimized. Updated renewable, price, load, equipment-availability, and production-progress observations define the root state. The first 15-minute action is implemented and the horizon then advances.

4.2.4. Real-Time Dispatch Model

The real-time dispatch model operates at a 10-minute interval and addresses rapid variations in renewable output and manufacturing electricity demand. Its objective is to minimize real-time operating cost and power-deviation penalty while preserving production feasibility.

The objective function is:

$$min\sum_{t=1}^{T_{\text{real}}}[C_{\text{ESS,real}}(t)+C_{\text{load,real}}(t)+C_{\text{dev,real}}(t)] \tag{7c}$$

In Equation (7c), min is the minimization operator; t is the real-time interval index; T_{real} is the number of real-time intervals and equals 144 for a 24-hour horizon with 10-minute resolution; $C_{\text{ESS,real}}(t)$ is the energy-storage operation and maintenance cost at interval t; $C_{\text{load,real}}(t)$ is the regulation cost of approved flexible manufacturing and utility loads; and $C_{\text{dev,real}}(t)$ is the penalty for deviation between scheduled and actual grid-exchange power. The subscript real identifies the real-time dispatch stage.

Because real-time decisions must be implemented rapidly, the model focuses on power balance and the operating limits of fast-response resources. Battery storage, compressed-air systems, industrial HVAC, charging facilities, and selected noncritical machines can adjust quickly, whereas critical and quality-sensitive processes remain fixed. This separation allows fluctuations to be suppressed without disrupting production.

The real-time model uses model predictive control. It receives smart-meter data, equipment states, and short-term renewable and load forecasts, predicts the next operating periods, solves the optimization problem, and executes only the current control action. Rolling prediction and correction provide rapid response while maintaining consistency with the manufacturing schedule.

4.2.5. Multi-Stage Coupling and Coordination

Coordination among the day-ahead, intraday, and real-time models is realized through data feedback and instruction transmission. The day-ahead energy plan is based on the production schedule, the intraday stage updates it using production progress and forecast information, and the real-time stage uses the revised plan as a baseline. Actual energy consumption and manufacturing status are then fed back to subsequent scheduling cycles.

For data feedback, intraday scheduling sends updated production-load forecasts, order information, and operating data to the next day-ahead cycle. Real-time scheduling returns power deviations, storage state, utility-system state, and production progress to the intraday optimizer, which updates its parameters and constraints.

For instruction transmission, the day-ahead plan is issued to the park energy-management and manufacturing-execution systems. Intraday optimization revises controllable-resource and flexible-load schedules, while real-time control sends executable commands to storage, utility systems, and approved noncritical production loads.

Coupling is enforced rather than described only procedurally. Storage, unit, and production states at the first intraday and real-time intervals equal the implemented terminal state of the preceding stage; sub-hourly energy aggregates to the relevant hourly commitment; and decisions inside the frozen production horizon cannot be revised:

$$SOC_{q_0}^{\text{ID}}=SOC_{h^*}^{\text{DA}};\quad SOC_{r_0}^{\text{RT}}=SOC_{q^*}^{\text{ID}} \tag{7d}$$

$$\sum_{q\in Q(h)}P_q^{\text{ID}}\Delta t^{\text{ID}}=P_h^{\text{DA}}\Delta t^{\text{DA}}+\delta_h^{\text{ID}} \tag{7e}$$

$$x_{\tau i,t}=\bar{x}_{i,t}\quad \text{for } t \text{ within the frozen horizon} \tag{7f}$$

Here h^* and q^* are the latest implemented day-ahead and intraday states, δ_h^{ID} is the permitted recourse deviation, and $\bar{x}$ is a released production or commitment decision. Together with node-wise non-anticipativity, Equations (7d)-(7f) prevent double scheduling of flexibility and maintain physical consistency across all three time scales.

4.3. Integration of Low-Carbon Manufacturing Targets and Demand Response

4.3.1. Development and Integration of Carbon Flow Calculation Model

The carbon boundary is operational and gate-to-gate. It includes Scope 1 emissions from on-site fuel use and location-based Scope 2 emissions from imported electricity. Embodied equipment emissions, upstream fuel-cycle emissions, and avoided-emission credits are outside the boundary. Renewable generation has zero operational carbon in the model; curtailment receives no negative credit. Each inflow carries a source-specific carbon intensity so that the same emission is counted once when energy is generated or imported and then traced to its final use [15,16].

For controllable distributed generators, carbon emissions are calculated based on fuel consumption and carbon emission factors:

$$E_{\text{DG}}(t)=\lambda_{\text{DG}}\times P_{\text{DG}}(t)\times\Delta t \tag{8}$$

In Equation (8), $E_{\text{DG}}(t)$ is the carbon emitted by controllable distributed generation during interval t, measured in kg; λ_{DG} is the generator carbon-emission factor in kg/kWh; $P_{\text{DG}}(t)$ is generator output power in kW; Δt is the interval duration in hours; and the subscript DG denotes distributed generation.

For purchased electricity, the embedded carbon emissions are calculated based on the average carbon emission factor of the power grid:

$$E_{\text{grid}}(t)=\lambda_{\text{grid}}\times P_{\text{grid,in}}(t)\times\Delta t \tag{9}$$

In Equation (9), $E_{\text{grid}}(t)$ is the embedded carbon emission of purchased grid electricity during interval t; λ_{grid} is the average grid carbon-emission factor in kg/kWh; $P_{\text{grid,in}}(t)$ is imported grid power in kW; Δt is the interval duration in hours; and the subscript in denotes electricity flowing into the manufacturing park.

Battery charging and discharging do not create direct emissions, but stored energy retains the carbon tag of its charging mix. Let M_t^{ES} be the carbon mass stored with electrical energy E_t^{ES}; $\lambda_t^{\text{ES}}=\frac{M_t^{\text{ES}}}{E_t^{\text{ES}}}$. Charging adds $\eta_{ch}\lambda_t^{in}P_t^{ch}\Delta t$ to the inventory, and discharging transfers $\frac{\lambda_t^{\mathrm{ES}} P_t^{\mathrm{dis}} \Delta t}{\eta_{\mathrm{dis}}}$ to the receiving load. Renewable curtailment is excluded from both energy and carbon inventories.

$$M_{t+1}^{\mathrm{ES}} = M_t^{\mathrm{ES}} + \eta_{\mathrm{ch}} \lambda_t^{\mathrm{in}} P_t^{\mathrm{ch}} \Delta t - \frac{\lambda_t^{\mathrm{ES}} P_t^{\mathrm{dis}} \Delta t}{\eta_{\mathrm{dis}}} \quad (10a)$$

$$\lambda_t^{\mathrm{ES}} = \frac{M_t^{\mathrm{ES}}}{E_t^{\mathrm{ES}}} \quad (10b)$$

For exported electricity, the sending park subtracts the exported source-tagged carbon flow from its internal allocation but does not claim negative emissions. For inter-park exchange $p \to q$, both energy and carbon tag $\lambda_{p\to q}$ are transferred; park q allocates the received carbon to its loads, while park p records the transfer once. Production or auxiliary load k receives $E_k = \sum_t \lambda_t^{\mathrm{bus}} P_{k,t} \Delta t$. These rules conserve carbon mass across generation, storage, exchange, export, and consumption and prevent double counting.

$$E_k = \sum_t \lambda_t^{\mathrm{bus}} P_{k,t} \Delta t; \quad E_{p\to q} = \sum_t \lambda_{p\to q,t} P_{p\to q,t} \Delta t \quad (10c)$$

Integrating the carbon flow calculation model into a multi-timescale regulation decision model involves adding a carbon emission minimization objective to the objective function and setting carbon emission constraints in the constraints:

$$\sum\nolimits_{t=1}^{T} [E_{\mathrm{DG}}(t) + E_{\mathrm{grid}}(t)] \le E_{\max} \quad (10)$$

In Equation (10), t is the dispatch-period index; T is the total number of periods; EDG(t) is the distributed-generator emission from Equation (8); Egrid(t) is the purchased-electricity emission from Equation (9); Σ accumulates emissions over all periods; Emax is the upper limit of the carbon emission budget, and the inequality ≤ constrains total operational emissions to stay below this budget. All emission terms use the same carbon-mass unit, kg in the case study.

4.3.2. Integration of Production-Aware Price-Based Demand Response

Production-aware price-based demand response uses time-of-use and real-time prices to guide the scheduling of shiftable processes and industrial utility systems. The model exploits manufacturing flexibility only within process, quality, delivery, and equipment constraints, thereby improving controllability without treating production demand as freely interruptible.

An electricity-price elasticity matrix describes the response of flexible manufacturing loads to price changes. Self-elasticity represents the change in a load during the same period, while cross-elasticity represents load transfer between periods. For production applications, the elasticity coefficients are applied only to loads and time windows approved by the production plan.

The load adjustment after demand response is calculated as:

$$\Delta P_{\mathrm{load}}(t) = \sum\nolimits_{s=1}^{T} \varepsilon_{\mathrm{ts}} \times P_{\mathrm{load,base}}(s) \times \frac{p(s) - p_{\mathrm{base}}(s)}{p_{\mathrm{base}}(s)} \quad (11)$$

In Equation (11), $\Delta P_{\mathrm{load}}(t)$ is the net flexible-load adjustment in response period t; s is the electricity-price-change period; T is the number of periods in the dispatch cycle; $\varepsilon_{\mathrm{ts}}$ is the price-elasticity-matrix element linking a price change in period s to a load response in period t; $P_{\mathrm{load,base}}(s)$ is baseline flexible load; $p(s)$ is the implemented price; $p_{\mathrm{base}}(s)$ is the baseline price; and $\frac{p(s) - p_{\mathrm{base}}(s)}{p_{\mathrm{base}}(s)}$ is the relative price change. For $t=s$, $\varepsilon_{\mathrm{ts}}$ is self-elasticity; for $t \neq s$, it is cross-elasticity.

Integrating the price-based demand response model into the multi-timescale regulation decision model involves considering demand response costs in the objective function and upper/lower limits on load adjustment quantities in the constraints:

$$-\Delta P_{\mathrm{load,max}}(t) \le \Delta P_{\mathrm{load}}(t) \le \Delta P_{\mathrm{load,max}}(t) \quad (12)$$

In Equation (12), $\Delta P_{\mathrm{load}}(t)$ is the adjustment defined by Equation (11); $\Delta P_{\mathrm{load,max}}(t)$ is the maximum permitted absolute adjustment; $-\Delta P_{\mathrm{load,max}}(t)$ is the lower bound; $+\Delta P_{\mathrm{load,max}}(t)$ is the upper bound or rebound limit; and the two ≤ signs impose a symmetric feasible interval. A negative $\Delta P_{\mathrm{load}}(t)$ denotes load reduction or postponement, whereas a positive value denotes load increase or recovery.

The demand-response model is coordinated with dispatch planning. At the day-ahead stage, shiftable production and utility-load strategies are formulated from the electricity-price forecast and production schedule. Intraday and real-time stages revise only the remaining feasible flexibility according to updated prices, equipment status, and production progress.

4.3.3. Process-Feasibility and Rebound Constraints

For process j and period t, y_{jt}, u_{jt}, and z_{jt} denote operating, start-up, and interruption binaries; a_{jt} is equipment availability; S_j and C_j are start and completion times; d_j is the delivery deadline; L_j is minimum continuous run time; I_j^{max} is the maximum number of interruptions; and s_{ij} is setup time between predecessor i and successor j. The following constraints are enforced in every scenario:

$$y_{jt} \le a_{jt}; \quad u_{jt} \ge y_{jt} - y_{j,t-1} \quad (12a)$$

$$C_i + s_{ij} \le S_j; \quad C_j \le d_j \quad (12b)$$

$$\sum_{\tau=t}^{t+L_j-1} y_{j\tau} \ge L_j u_{jt} \quad (12c)$$

$$\sum_t z_{jt} \le I_j^{\max}; \quad z_{jt} \ge y_{j,t-1} - y_{jt} \quad (12d)$$

$$\sum_{t\in W_j} P_{jt} \Delta t = E_j^{\mathrm{req}}; \quad P_{j,\min} y_{jt} \le P_{jt} \le P_{j,\max} y_{jt} \quad (12e)$$

$$\sum_{t\in R_j} \Delta P_{jt} \Delta t = 0; \quad \left|\Delta P_{jt}\right| \le \Delta P_{j,\max} \quad (12f)$$

Equation (12a) prevents operation during equipment unavailability and identifies starts; Equation (12b) enforces sequence, setup, and delivery; Equation (12c) enforces minimum uninterrupted operation; Equation (12d) limits interruption count; Equation (12e) preserves required production energy and operating bounds; and Equation (12f) forces curtailed energy to rebound inside an approved recovery window R_j rather than disappearing. Shared-machine disjunctive constraints prevent overlapping jobs. Critical and quality-sensitive processes are fixed, while only approved shiftable processes and utility systems participate in demand response.

4.4. Multi-Manufacturing-Park Collaborative Dispatch Mechanism

A multi-park MP-VPP system improves resource allocation through coordinated electricity exchange, reserve sharing, and complementary production-load profiles. The collaborative objective is to minimize total operating cost and carbon emissions while satisfying each park's production and confidentiality constraints.

The mechanism includes day-ahead collaborative planning, in which each park reports available energy resources and aggregated flexibility; intraday collaborative adjustment, in which updated forecasts and production changes are coordinated; and real-time collaborative response, in which fast resources jointly balance short-term deviations. Detailed process data remain at the local park level, while only necessary flexibility information is shared.

An industrial-internet platform supports forecasts, operating status, dispatch instructions, and energy-exchange information [7,28]. A benefit-allocation mechanism distributes collaborative gains according to each park's contribution, encouraging participation while maintaining data security and operational autonomy.

5. Manufacturing-Park Case Study Simulation and Validation

5.1. Case Study Setup

5.1.1. System Parameters

The case study considers two manufacturing-park virtual power plants. Each park contains wind and photovoltaic generation, a gas turbine, lithium-ion battery storage, industrial utility loads, charging facilities, and selected shiftable production loads. Critical production demand is treated as noninterruptible, while flexible loads are scheduled within permitted operating windows. The principal system parameters are as follows:

Gas turbine parameters: Maximum output 500 kW, minimum output 0 kW, maximum ramp rate 230 kW/h, minimum ramp rate −220 kW/h, quadratic fuel-cost coefficient a=0.002 CNY/(kW·h)^2, linear coefficient b=0.3 CNY/(kW·h), start-up and shutdown costs 1.98 CNY and 1.32 CNY, respectively, and carbon-emission factor 0.8 kg/kWh. The variables a and b are the quadratic and linear coefficients of the gas-turbine fuel-cost function.

Energy Storage System Parameters: Rated capacity: 420 kWh Initial energy storage: 150 kWh Charging/discharging efficiency: 0.98 Maximum charging/discharging power: 200 kW State of charge (SOC) upper limit: 0.9 State of charge (SOC) lower limit: 0.1 Operational maintenance cost: 15.9 CNY/(kW • h)

Wind Power Parameters: Maximum output 300 kW, Weibull shape parameter k=2.5, and scale parameter c=180 kW. The parameter c is the fitted scale parameter used in the case study and corresponds to the symbol l in Equation (2).

Photovoltaic Parameters: Maximum output 200 kW, with beta-distribution shape parameters α=2.8 and β=3.2. In the case study, α and β correspond to m and n, respectively, in Equation (3).

Flexible Manufacturing Load Parameters: the total adjustable industrial utility load is 400 kW, including compressed-air and HVAC systems, and the total shiftable production-load capacity is 300 kW. The electricity-price elasticity matrix uses a self-elasticity coefficient of -0.3 and a cross-elasticity coefficient of 0.05. Regulation cost coefficients remain consistent with the original model assumptions.

Electricity Price Parameters: Daily electricity prices are set from the case-study tariff. Peak-period (09:00-12:00 and 17:00-21:00) rates are 1.10 CNY/kWh, flat-period (07:00-09:00, 12:00-17:00, and 21:00-22:00) rates are 0.66 CNY/kWh, and valley-period (00:00-07:00 and 22:00-24:00) rates are 0.35 CNY/kWh. Day-ahead and real-time prices are updated according to supply-demand conditions.

Carbon Emission Parameters: The average carbon emission factor for the power grid is 0.6 kg/kWh, and the carbon trading price is 50 CNY/kg.

5.1.2. Data, Scenario, and Solver Settings

The data interface requires, for each park and timestamp, forecast and realized wind/PV output, critical and flexible load, production order, process progress, equipment availability, electricity price, and grid carbon factor. Records are aligned to the dispatch clock, missing values are flagged rather than silently interpolated, and capacities are reported in physical units. To permit release without exposing commercially sensitive production volumes, the final data package should also provide each 24-hour profile normalized by the corresponding rated capacity or peak demand together with the scaling constants used in the tables.

Each day-ahead run generates 1,000 joint scenarios and retains 10; each intraday update retains 6 conditional scenarios; and each real-time update retains 5. Retained probabilities are computed from cluster membership as described in Section 3.3 and must be reported beside the trajectories. The optimization is formulated as a mixed-integer quadratic program. All benchmark runs use the same Gurobi 11.0 settings: relative MIP gap 0.1%, maximum wall-clock time 1,800 s, and deterministic seed 2026. Convergence is declared only when the gap criterion is met; otherwise the incumbent objective, final gap, and runtime are reported.

5.1.3. Benchmark and Simulation Scenario Design

Five benchmark configurations are defined using identical input profiles, capacities, carbon factors, solver tolerances, and production obligations:

B1—Deterministic single-time-scale baseline: point forecasts and day-ahead scheduling only; this is the original Scenario 1.

B2—Conventional stochastic multi-time-scale dispatch: probability-weighted scenarios and three-stage recourse, but generic elastic demand and no process-level or source-tagged carbon constraints.

B3—Budgeted robust multi-time-scale dispatch: the same three stages with a box/budget uncertainty set and worst-case objective, calibrated to the 95% marginal error intervals.

B4—Literature-based multi-time-scale MPC benchmark: rolling renewable/storage/grid tracking with generic flexible loads, following the rolling-planning and model-predictive-control information structures in [4,5,26] but using the present case data and objective coefficients.

B5—Proposed data-model hybrid method: validated distributions, probability-weighted scenarios, full stage coupling, process-feasibility constraints, source-tagged carbon flow, and multi-park coordination; this is the original Scenario 2.

All configurations are evaluated over the same 24-hour horizon using operating cost, total operational carbon, renewable-energy absorption, power-fluctuation standard deviation, process-feasibility rate, runtime, and final optimality gap. The supplied manuscript contains verified numerical outputs for B1 and B5 and for independent versus collaborative operation; B2-B4 must be rerun from the authors' source data and code before submission. No intermediate benchmark values are inferred or fabricated in this revision.

5.2. Simulation Results and Analysis

5.2.1. Operating Cost Analysis

Table 1 compares the five operating-cost components and the total cost of the two scenarios. Although Scenario 2 introduces a flexible-manufacturing-load regulation cost of ¥789.3, it reduces fuel cost by ¥1,327.8, storage operating cost by ¥189.0, electricity purchase/sale cost by ¥1,280.5, and deviation-penalty cost by ¥3,388.5 relative to Scenario 1. Consequently, the total operating cost decreases from ¥23,910.0 to ¥18,513.5, corresponding to a 22.6% reduction. The results in Table 1 show that the additional demand-response expenditure is more than offset by improved renewable utilization, storage coordination, and intraday and real-time deviation correction.

Table 1. Comparison of Operating Costs across Scenarios (Unit: ×10³ CNY)

S	F	ESS	Flex	Grid	Dev	Tot
S1	8.6	1.2	0	10.3	3.8	23.9
S2	7.2	1.1	0.8	9.0	0.5	18.5

Table 1 notation: F = fuel; ESS = energy storage; Flex = flexible-load regulation; Grid = electricity purchase/sale; Dev = deviation penalty; Tot = total operating cost. Values are expressed in ×10³ CNY and rounded to one decimal; exact values are given in the accompanying text.

5.2.2. Carbon Emissions Analysis

Table 2 reports gas-turbine emissions, the embedded emissions of purchased electricity, total carbon emissions, and the corresponding carbon cost. Scenario 2 reduces gas-turbine emissions from 6,852.4 kg to 5,468.2 kg and purchased-electricity emissions from 5,789.3 kg to 4,895.6 kg. Total emissions therefore fall by 2,277.9 kg, from 12,641.7 kg to 10,363.8 kg, while carbon cost decreases from ¥63,208.5 to ¥51,819.0. These results confirm that the carbon-flow objective shifts dispatch toward renewable consumption and away from high-carbon grid purchases and gas-turbine generation.

Table 2. Comparison of Carbon Emissions Across Scenarios (Unit: kg)

Scenario	Gas Turbine Carbon Emissions	Purchased-Electricity Emissions	Total Carbon Emissions	Carbon Emission Cost
Scenario 1	6,852.4	5,789.3	12,641.7	63,208.5
Scenario 2	5,468.2	4,895.6	10,363.8	51,819.0

5.2.3. Analysis of New Energy Integration Rate

Table 3 compares the wind-power, photovoltaic, and overall renewable-energy absorption rates. Scenario 2 increases wind-power absorption from 82.5% to 94.2% and photovoltaic absorption from 85.3% to 95.6%, yielding an overall absorption rate of 94.8%, which is 11.1 percentage points higher than Scenario 1. The component-level results in Table 3 indicate that reserving storage and load flexibility in the day-ahead stage, revising the plan intraday, and absorbing residual fluctuations in real time jointly improve the utilization of both renewable sources.

Table 3. Comparison of Renewable Energy Integration Rates Across Different Scenarios (Unit: %)

Scenario	Wind Power Absorption Rate	PV Absorption Rate	Total Absorption Rate
Scenario 1	82.5	85.3	83.7
Scenario 2	94.2	95.6	94.8

5.2.4. Power Fluctuation Suppression Analysis

Table 4 presents the power-fluctuation standard deviation in the day-ahead, intraday, real-time, and overall periods. Compared with Scenario 1, Scenario 2 reduces the day-ahead value from 125.6 kW to 92.3 kW, the intraday value from 156.8 kW to 85.6 kW, and the real-time value from 189.3 kW to 68.9 kW. The overall standard deviation decreases from

160.5 kW to 82.2 kW, a reduction of 48.8%. The especially large real-time improvement shown in Table 4 demonstrates that battery storage and fast industrial utility loads effectively suppress short-duration fluctuations and improve power quality for sensitive manufacturing equipment.

Table 4. Comparison of Power Fluctuation Standard Deviation Across Scenarios (Unit: kW)

Scenario	Day-ahead Period	Intraday Period	Real-time Period	Overall
Scenario 1	125.6	156.8	189.3	160.5
Scenario 2	92.3	85.6	68.9	82.2

5.2.5. Analysis of Collaborative Effects Across Manufacturing Parks

Table 5 compares independent dispatch with collaborative scheduling across the two manufacturing parks. Collaborative scheduling lowers total operating cost from ¥21,356.8 to ¥18,513.5 and total carbon emissions from 11,895.3 kg to 10,363.8 kg, while increasing renewable-energy absorption from 90.2% to 94.8% and reducing power-fluctuation standard deviation from 98.5 kW to 82.2 kW. Thus, as shown in Table 5, multi-park coordination achieves cost and emission reductions of 13.3% and 12.9%, respectively, by exploiting complementary production-load profiles and sharing flexible resources without violating local process constraints.

Table 5. Performance Metrics Comparison between Collaborative and Independent Dispatch

Dispatch Method	Total Operating Cost (CNY)	Total Carbon Emissions (kg)	Total Renewable Energy Absorption Rate (%)	Power Fluctuation Standard Deviation (kW)
Independent Dispatch	21,356.8	11,895.3	90.2	98.5
Collaborative Scheduling	18,513.5	10,363.8	94.8	82.2

5.2.6. Mechanism, Theoretical Contribution, and Engineering Implications

The cost reduction is driven mainly by recourse rather than by load curtailment. Day-ahead scheduling reserves storage headroom and process slack; intraday optimization reallocates those reserves after forecast and order updates; and real-time control removes the remaining mismatch. This sequence explains why the largest cost decrease occurs in deviation penalties and why fluctuation suppression is strongest at the real-time scale. The carbon decrease arises because source-tagged accounting makes high-carbon grid purchases and gas generation visible at the consuming process, while storage shifts low-carbon energy without erasing its original carbon intensity.

The theoretical contribution is the interface between uncertainty evidence and executable manufacturing decisions: fitted distributions produce probability-weighted trajectories; the coupled optimization converts those trajectories into feasible energy and production actions; and realized states update the next fitting and recourse cycle. The process constraints narrow the nominal flexibility but prevent solutions that would save energy cost by violating sequence, minimum run time, quality, or delivery obligations. Therefore, economic and carbon improvements are interpreted only within the process-feasible region.

For engineering deployment, the day-ahead layer exchanges hourly commitments with the energy-management and manufacturing-execution systems, the intraday layer updates not-yet-released work orders and utility set points, and the real-time layer controls only approved fast resources. Inter-park coordination shares aggregated flexibility and carbon-tagged energy rather than proprietary process details. The minimum implementation requirements are synchronized timestamps, equipment-availability flags, auditable carbon factors, a rollback rule for failed optimization, and local safety interlocks that override dispatch commands.

5.3. Sensitivity Analysis

Sensitivity analysis is conducted on four parameters: wind-power fluctuation, photovoltaic-output fluctuation, manufacturing-load fluctuation, and carbon-trading price. Each parameter varies by ±20% to evaluate changes in total operating cost and carbon emissions.

5.3.1. Sensitivity Analysis of Wind Power Output Fluctuation Coefficient

Figure 5 shows that both total operating cost and total carbon emissions increase almost linearly as the wind-power output fluctuation coefficient rises from 0.8 to 1.2. Relative to the nominal coefficient of 1.0, increasing the coefficient to 1.2 raises operating cost by ¥1,256.8 (6.8%) and carbon emissions by 895.6 kg (8.6%). The trend in Figure 5 indicates that stronger wind-power uncertainty requires more balancing energy and greater use of dispatchable resources, with carbon emissions responding more strongly than operating cost.

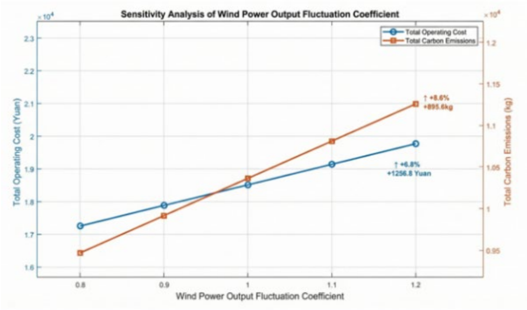

Figure 5. Sensitivity analysis of the wind-power output fluctuation coefficient

5.3.2. Sensitivity Analysis of PV Output Fluctuation Coefficient

Figure 6 shows a monotonic increase in both total operating cost and total carbon emissions as the photovoltaic-output fluctuation coefficient rises. When the coefficient increases from the nominal value of 1.0 to 1.2, operating cost increases by ¥876.3 (4.7%) and carbon emissions increase by 654.2 kg (6.3%). The results in Figure 6 demonstrate that photovoltaic uncertainty reduces the effectiveness of renewable-energy scheduling and increases the need for grid purchases and controllable generation.

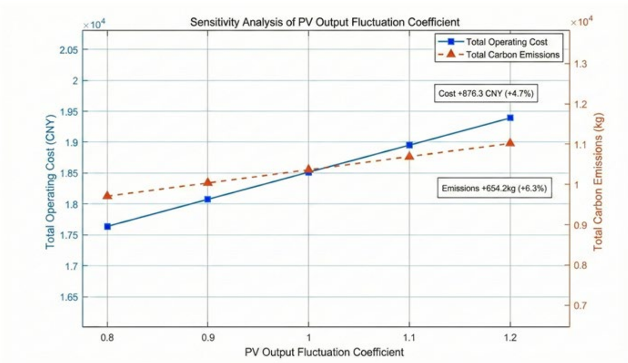

Figure 6. Sensitivity analysis of the photovoltaic-output fluctuation coefficient

5.3.3. Manufacturing Load Fluctuation Coefficient Sensitivity Analysis

Figure 7 illustrates that manufacturing-load uncertainty has a clear adverse effect on both economic and low-carbon performance. When the load-fluctuation coefficient increases from 1.0 to 1.2, total operating cost rises by ¥1,056.2 (5.7%) and total carbon emissions rise by 789.3 kg (7.6%). The steeper carbon-emission curve in Figure 7 indicates that inaccurate production-load forecasts can rapidly consume the low-carbon scheduling margin and require additional high-carbon balancing resources.

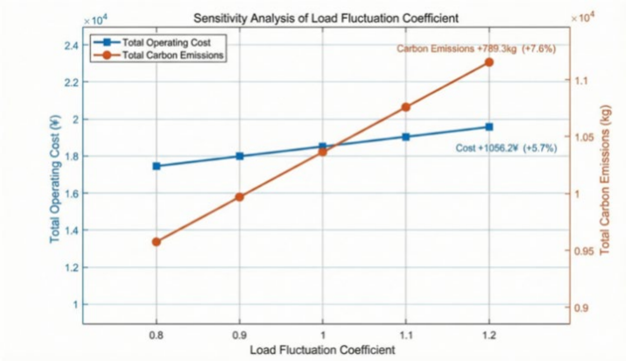

Figure 7. Sensitivity analysis of the manufacturing-load fluctuation coefficient

5.3.4. Carbon Trading Price Sensitivity Analysis

Figure 8 presents opposite trends for operating cost and carbon emissions as the carbon-trading price increases from 40 to 60 RMB/kg. Total operating cost rises nearly linearly because high-emission generation and grid purchases become more expensive, whereas total carbon emissions decline continuously as the optimizer shifts toward renewable energy, storage, and flexible-load regulation. The trade-off shown in Figure 8 confirms that a higher carbon price strengthens the economic incentive for low-carbon dispatch, although it also increases the direct operating expenditure of the manufacturing parks.

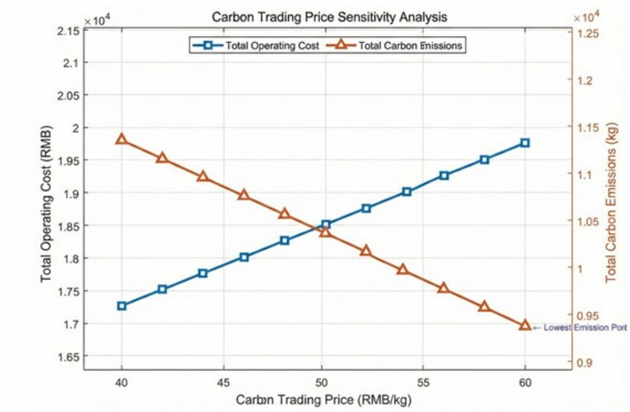

Figure 8. Sensitivity analysis of the carbon-trading price

6. Conclusions and Outlook

6.1. Research Conclusions

Manufacturing parks are moving toward integrated production-energy management because energy cost and carbon intensity increasingly affect operational competitiveness. Their heterogeneous loads also provide dispatch flexibility, provided that process continuity and product-quality constraints are preserved. This paper develops a multi-timescale regulation decision model for manufacturing-park virtual power plants and draws the following conclusions:

The resource structure and multi-timescale dispatch characteristics of MP-VPPs are clarified. Day-ahead, intraday, and real-time objectives, time granularities, and constraints are defined together with production continuity, process sequence, and flexible-load windows, forming a manufacturing-oriented dispatch framework.

A multi-timescale uncertainty model is established for wind power, photovoltaic output, manufacturing load, and electricity price. Weibull, beta, and normal distributions together with scenario generation and reduction provide representative inputs for production-energy scheduling.

The optimized three-stage model now specifies probability-weighted day-ahead planning, intraday recourse, real-time tracking, inter-stage state continuity, and process-feasibility constraints. Source-tagged carbon accounting covers purchased electricity, storage, curtailment, export, and inter-park exchange. For the verified B1/B5 comparison in the supplied case, the method reduces operating cost by 22.6%, lowers operational carbon by 18.0%, raises renewable-energy absorption to 94.8%, and reduces power-fluctuation standard deviation by 48.8% while maintaining production feasibility. Sensitivity analysis confirms robustness to renewable-output, manufacturing-load, and carbon-price changes. Collaborative dispatch across manufacturing parks further improves resource utilization by combining complementary production profiles, storage capability, and industrial utility flexibility.

6.2. Research Outlook

The results provide a technical reference for multi-timescale energy management in manufacturing parks, but three limitations delimit the present evidence. First, the production response still aggregates some utility and process behavior despite the added feasibility constraints. Second, site-level input records are commercially sensitive and must be released as normalized profiles for independent numerical replication. Third, the deterministic, stochastic, robust, and MPC benchmark definitions introduced in Section 5.1.3 require final reruns from the authors' source data before resubmission. These limitations motivate the following research directions:

Further Optimization of Uncertainty Quantification Methods: The probabilistic distribution model employed in this study relies on historical data statistics and does not fully account for the impact of extreme weather conditions and unforeseen events. Future work could integrate machine learning methods, such as long short-term memory networks or random forests, to enhance the accuracy of uncertainty prediction and develop more precise uncertainty quantification models.

Expansion of Multi-Energy Coordinated Dispatch: Future work should include electricity, steam, heat, gas, chilled water, and compressed air, as these energy carriers are strongly coupled with manufacturing processes. A multi-energy MP-VPP model could coordinate production scheduling and utility-system operation to improve overall efficiency.

Application of Blockchain Technology in multi-park MP-VPP Coordination: Information security and trust mechanisms are critical in multi-park MP-VPP coordination. Future research could introduce blockchain technology to build decentralized information sharing and transaction platforms, ensuring information security and transaction transparency. This would optimize benefit distribution mechanisms, enhancing the efficiency and reliability of multi-park MP-VPP coordination.

Production-Flexibility Models Considering Operational Uncertainty: The current elasticity-based demand-response model simplifies the relationship between production behavior and electricity prices. Future work should represent uncertain order arrival, machine failure, setup time, product quality, and operator intervention to improve the accuracy and implementability of manufacturing-load regulation.

As smart manufacturing and low-carbon industrial transformation advance, MP-VPPs can become an important interface between factory production systems and the power market. Future studies should strengthen data-driven forecasting, process-level flexibility modeling, and secure industrial-internet coordination to support large-scale engineering application.

Acknowledgements

This work was supported by the project "Technical consulting services for the scheme of enhancing the power support capacity and upgrading the flexible interaction capability of microgrids with a high proportion of renewable energy in the Hebei Southern Power Grid" (Project No. B704JY220058).

References

[1] Pudjianto D, Ramsay C, Strbac G. Virtual power plant and system integration of distributed energy resources. IET Renewable Power Generation. 2007;1(1):10-16.

[2] Ruan G, Qiu D, Sivaranjani S, Awad A S A, Strbac G. Data-driven energy management of virtual power plants: A review. Advances in Applied Energy. 2024;14:100170.

[3] Pandžić H, Morales J M, Conejo A J, Kuzle I. Offering model for a virtual power plant based on stochastic programming. Applied Energy. 2013;105:282-292.

[4] Luo F J, Dong Z Y, Meng K, Qiu J, Yang J, Wong K P. Short-term operational planning framework for virtual power plants with high renewable penetrations. IET Renewable Power Generation. 2016;10(5):623-633.

[5] Parisio A, Rikos E, Glielmo L. A model predictive control approach to microgrid operation optimization. IEEE Transactions on Control Systems Technology. 2014;22(5):1813-1827.

[6] Jin X, Wu J, Mu Y, Wang M, Xu X, Jia H. Hierarchical microgrid energy management in an office building. Applied Energy. 2017;208:480-494.

[7] Shi W, Cao J, Zhang Q, Li Y, Xu L. Edge computing: Vision and challenges. IEEE internet of things journal, 2016;3(5):637-646.

[8] Bunse K, Vodicka M, Schönsleben P, Brülhart M, Ernst F O. Integrating energy efficiency performance in production management: Gap analysis between industrial needs and scientific literature. Journal of Cleaner Production. 2011;19(6-7):667-679.
[9] May G, Barletta I, Stahl B, Taisch M. Energy management in production: A novel method to develop key performance indicators for improving energy efficiency. Applied Energy. 2015;149:46-61.
[10] Pinson P, Girard R. Evaluating the quality of scenarios of short-term wind power generation. Applied Energy. 2012;96:12-20.
[11] Ju L, Tan Z, Yuan J, Tan Q, Li H, Dong F. A bi-level stochastic scheduling optimization model for a virtual power plant connected to a wind-photovoltaic-energy storage system considering the uncertainty and demand response. Applied Energy. 2016;171:184-199.
[12] Chen N, Qian Z, Nabney I T, Meng X. Wind power forecasts using Gaussian processes and numerical weather prediction. IEEE Transactions on Power Systems. 2014;29(2):656-665.
[13] Zhao C, Guan Y. Unified stochastic and robust unit commitment. IEEE Transactions on Power Systems. 2013;28(3):3353-3361.
[14] Dupačová J, Gröwe-Kuska N, Römisch W. Scenario reduction in stochastic programming: An approach using probability metrics. Mathematical Programming. 2003;95:493-511.
[15] Kang C, Zhou T, Chen Q, Wang J, Sun Y, Xia Q, Yan H. Carbon emission flow from generation to demand: A network-based model. IEEE Transactions on Smart Grid. 2015;6(5):2386-2394.
[16] Hawkes A D. Estimating marginal CO2 emissions rates for national electricity systems. Energy Policy. 2010;38(10):5977-5987.
[17] Wei X, Xu Y, Sun H, Bai X, Chang X, Xue Y. Day-ahead optimal dispatch of a virtual power plant in the joint energy-reserve-carbon market. Applied Energy. 2024;356:122459.
[18] Liu D, Xiao F, Wu J, Ji X, Xiong P, Zhang M, Kang Y. Electricity-carbon joint trading of virtual power plant with carbon capture system. International Transactions on Electrical Energy Systems. 2023;2023:6864403.
[19] Zhu R, Guan X, Zheng J, Wang N, Jiang H, Cui C, Ohtsuki T. DRL based low carbon economic dispatch by considering power transmission safety limitations in internet of Energy. Internet of Things. 2023;24:100979.
[20] Albadi M H, El-Saadany E F. Demand response in electricity markets: An overview. In: 2007 IEEE Power Engineering Society General Meeting; 2007. p. 1-5.
[21] Mohsenian-Rad A H, Wong V W S, Jatskevich J, Schober R, Leon-Garcia A. Autonomous demand-side management based on game-theoretic energy consumption scheduling for the future smart grid. IEEE Transactions on Smart Grid. 2010;1(3):320-331.
[22] Vasirani M, Kota R, Cavalcante R L G, Ossowski S, Jennings N R. An agent-based approach to virtual power plants of wind power generators and electric vehicles. IEEE Transactions on Smart Grid. 2013;4(3):1314-1322.
[23] Liu N, Yu X, Wang C, Li C, Ma L, Lei J. Energy-sharing model with price-based demand response for microgrids of peer-to-peer prosumers. IEEE Transactions on Power Systems. 2017;32(5):3569-3583.
[24] Tan Z F, Li H H, Ju L W, Tan Q K. Joint scheduling optimization of virtual power plants and equitable profit distribution using Shapely value theory. Mathematical Problems in Engineering. 2018;2018:3810492.
[25] Geidl M, Andersson G. Optimal power flow of multiple energy carriers. IEEE Transactions on Power Systems. 2007;22(1):145-155.
[26] Li Q, Zhou Y, Wei F, et al. Multi-time scale scheduling for virtual power plants: Integrating the flexibility of power generation and multi-user loads while considering the capacity degradation of energy storage systems. Applied Energy. 2024;362:122980.
[27] Zhang X, Liu Y. Two-stage stochastic robust optimal scheduling of virtual power plant considering source-load uncertainty. Engineering Reports. 2024;6(12):e13005.
[28] Wicaksono H, Trat M, Bashyal A, et al. Artificial-intelligence-enabled dynamic demand response system for maximizing the use of renewable electricity in production processes. International Journal of Advanced Manufacturing Technology. 2025;138:247-271.